Electron tunnelling in a double ferromagnetic junction with a magnetic dot as a spacer

2002 J. Phys.: Condens. Matter 14 2011

(http://iopscience.iop.org/0953-8984/14/8/328)

INSTITUTE OF PHYSICS PUBLISHING JOURNAL OF PHYSICS: CONDENSED MATTER

J. Phys.: Condens. Matter **14** (2002) 2011–2023 PII: S0953-8984(02)28164-3

Electron tunnelling in a double ferromagnetic junction with a magnetic dot as a spacer

R Świrkowicz[1], **J Barnaś**[2,3] **and M Wilczyński**[1]

[1] Faculty of Physics, Technical University, ul. Koszykowa 75, 00-662 Warszawa, Poland
[2] Department of Physics, Adam Mickiewicz University, ul. Umultowska 85, 61-614 Poznań, Poland
[3] Institute of Molecular Physics, Polish Academy of Sciences, ul. M Smoluchowskiego 17, 60-179 Poznań, Poland

E-mail: barnas@spin.amu.edu.pl

Received 23 August 2001, in final form 26 October 2001
Published 15 February 2002
Online at stacks.iop.org/JPhysCM/14/2011

Abstract

Electron tunnelling in a double-barrier junction with ferromagnetic external electrodes and a magnetic quantum dot as a spacer is analysed theoretically in the framework of the nonequilibrium Green function technique. The considerations are restricted to spin-conserving tunnelling processes through a quantum dot with a single spin-split discrete level. The Coulomb correlations on the dot are taken into account in terms of the Hubbard Hamiltonian. Transport characteristics, including tunnelling magnetoresistance due to rotation of the magnetic moments of external electrodes, are calculated selfconsistently.

1. Introduction

Recent interest in spin-polarized tunnelling is stimulated by expected applications in magnetoelectronics and/or spintronics [1, 2]. This applies particularly to the tunnel magnetoresistance (TMR) effect. By applying a weak magnetic field, one can rotate magnetic moments of ferromagnetic electrodes from antiparallel (AP) to parallel (P) alignment, and this rotation is usually accompanied by a drop in the junction resistance [3, 4]. The effect is similar to the giant magnetoresistance effect discovered a decade ago in metallic magnetic multilayers [5, 6].

The TMR effect exists in simple planar junctions as well as in more complex ones, including planar [7] and mesoscopic [8–10] double-barrier junctions, granular systems [11, 12], etc. When the central electrode of a double-barrier junction is small, the corresponding capacitance C can be small as well. One can then easily reach the range where the charging energy, $E_c = e^2/2C$, is larger than the thermal energy $k_B T$. If this is the case, the effects due to discrete charging of the central electrode with single electrons modify the junction characteristics and lead to Coulomb blockade of electric current below a certain threshold

voltage and to characteristic Coulomb staircase above [13]. Additional features of electron tunnelling in mesoscopic double-barrier junctions are due to size quantization of electron states in the central electrode (referred to as a dot in the following) [14, 15].

In this paper we consider spin-polarized electron tunnelling through a quantum dot with a single spin-split discrete level. The work differs substantially from earlier publications on spin-polarized tunnelling in magnetic mesoscopic double-barrier junctions. Generally, the earlier works can be classified into three groups with respect to the model considered. The first group includes the papers, where the central electrode was a metallic grain with a high density of states at the Fermi level, so the effects due to size quantization were irrelevant and were not taken into account [8–10]. Addition of one extra electron costs then only the classical charging energy, $E_c = e^2/2C$. The second group includes the works concerning spin polarized transport in systems with the metallic central electrode being small enough to support discrete energy levels. The distance between the levels, however, was much smaller then the classical charging energy E_c. Addition of an extra electron requires than not only the charging energy, but also the energy related to the level separation, ΔE. Spin-polarized tunnelling in this limit ($\Delta E \ll E_c$) was considered quite recently [16]. Finally, the works where the charging effects are smaller than the effects due to size quantization, belong to the third category. This regime, however, was studied only in the limiting situation, where the quantum dot supports a single discrete level, and the Coulomb correlations are described by the Hubbard Hamiltonian (with the corresponding correlation parameter U playing the role of charging energy). To our knowledge, there are only two publications on spin polarized tunnelling in this limit [17, 18]. In [17] the case of infinite U and empty level in equilibrium was analysed within the master equation method. In a recent paper [18], the description based on the master equation was extended to the case of arbitrary value of the parameter U and also to arbitrary position of the discrete level. This paper is just a continuation of this work. First of all, we consider here a more general model. Second, we apply a significantly different technique, which is more accurate and applicable to a broader range of parameters. More precisely, the quantum dot is assumed here to be magnetic, with a spin-split discrete level, whereas in [18] the dot was nonmagnetic. The spin splitting of the level can be caused, for instance, by an external magnetic field or by coupling of the dot to a spin-polarized substrate. We show that such a splitting may lead to new effects like enhanced TMR and enhanced spin polarization of the tunnelling current. Moreover, in [18] the discrete level was assumed to shift linearly with applied bias, i.e. the effects due to charge accumulated on the dot were neglected. Such a description, however, is generally not gauge invariant. Therefore, in this work we use a gauge invariant approach, introduced recently to describe tunelling through single-level nonmagnetic dots [19]. Apart from this, in [18] the transport characteristics were calculated within the master equation technique. Such a description is valid when the thermal energy is much larger than the level width Γ, $kT \gg \Gamma$ [20]. In this paper, on the other hand, we use the technique based on the nonequilibrium Green functions [21–25]. This technique is more general—it also describes coherent tunnelling and takes into account the correlations on the dot in a more accurate way. Such a description requires self-consistent numerical calculations of the Green functions, occupation numbers and electrostatic potential of the dot. The Green functions are calculated in the Hartree–Fock approximation, so the description is valid above the Kondo temperature. At lower temperatures, however, one should calculate the Green functions more accurately, by taking into account many-body effects. The Kondo effect in quantum dots was predicted theoretically long time ago [26], and observed experimentally quite recently [27].

In general, the two external electrodes of the system under consideration and the quantum dot may be magnetic. Such a general case offers several possiblities for magnetic configuration.

Therefore, we will restrict our numerical calculations to two situations: (i) the case where the external electrodes are ferromagnetic and the dot is nonmagnetic, and (ii) the case when the dot and one of the external electrodes are magnetic, whereas the second external electrode is nonmagnetic. In each case two magnetic configurations will be analysed, i.e. the P and AP ones.

In section 2 we describe the model and analyse the general situation. Numerical results on tunnelling current and magnetoresistance are shown in section 3. Summary and final conclusions are presented in section 4.

2. Description of the model

The double-barrier junction considered in this paper consists of a small central part (quantum dot) which is coupled to two ferromagnetic leads (electrodes) by tunnelling barriers. The quantum dot is so small, that only a single discrete level is active in the tunnelling processes. Generally, the dot may be magnetic, so the discrete level is spin dependent.

Tunnelling current depends on relative orientation of the magnetic moments of external electrodes. Since the amplitude of TMR corresponds to the rotation from AP to P alignment, we simplify the problem by considering only these two magnetic configurations.

To describe electronic transport, we describe the system by the following model Hamiltonian:

$$H = H_{\mathrm{l}} + H_{\mathrm{r}} + H_{\mathrm{d}} + H_{\mathrm{t}}. \tag{1}$$

Here, H_{l} and H_{r} describe the left and right electrodes in the noninteracting particle limit,

$$H_{\alpha} = \sum_{nk\sigma} \epsilon^{\alpha}_{nk\sigma} a^{+}_{\alpha nk\sigma} a_{\alpha nk\sigma} \tag{2}$$

for $\alpha = l$ and r, where $\epsilon^{\alpha}_{nk\sigma}$ is the single-electron energy in the electrode α for the one-dimensional wavevector k, channel n and spin σ ($\sigma = \uparrow, \downarrow$), whereas $a^{+}_{\alpha nk\sigma}$ and $a_{\alpha nk\sigma}$ are the relevant creation and destruction operators. The energy $\epsilon^{\alpha}_{nk\sigma}$ includes the electrostatic energy,

$$\epsilon^{\alpha}_{nk\sigma} = \epsilon^{0\alpha}_{nk\sigma} + eU^{\alpha}_{\mathrm{e}} \tag{3}$$

where U^{α}_{e} is the electrostatic potential of the αth electrode, e is the electron charge, and $\epsilon^{0\alpha}_{nk\sigma}$ is the single-electron energy at vanishing electrostatic potential. In the following we assume that for negative bias the left (right) electrode is the source (drain) one, so $U^{\mathrm{l}}_{\mathrm{e}} < U^{\mathrm{r}}_{\mathrm{e}}$ ($e < 0$).

The term H_{d} in the Hamiltonian (1) describes the dot and is of the Hubbard form,

$$H_{\mathrm{d}} = \sum_{\sigma} E_{\sigma} c^{+}_{\sigma} c_{\sigma} + U c^{+}_{\uparrow} c_{\uparrow} c^{+}_{\downarrow} c_{\downarrow} \tag{4}$$

where E_{σ} is the spin-dependent energy of the discrete level and U is the electron correlation parameter. The energy E_{σ} of the discrete level can be written as [19]

$$E_{\sigma} = E^{0}_{\sigma} + eU_{\mathrm{e}} \tag{5}$$

where E^{0}_{σ} is the level energy at zero bias and U_{e} is the electrostatic potential of the dot. We assume that U_{e} can be calculated from a simple capacitive model [19]:

$$e\left(\sum_{\sigma} n_{\sigma} - \sum_{\sigma} n_{0\sigma}\right) = C_{\mathrm{l}}(U_{\mathrm{e}} - U^{\mathrm{l}}_{\mathrm{e}}) + C_{\mathrm{r}}(U_{\mathrm{e}} - U^{\mathrm{r}}_{\mathrm{e}}) \tag{6}$$

where n_{σ} are the occupation numbers, $n_{\sigma} = \langle c^{+}_{\sigma} c_{\sigma} \rangle$, $n_{0\sigma}$ are these numbers at zero bias, whereas C_{l} and C_{r} denote the left and right junction capacitances.

The last term, H_t, in equation (1) stands for the tunnelling part of the Hamiltonian, and may be written as

$$H_t = \sum_{nk\sigma} T^l_{nk\sigma} a^+_{lnk\sigma} c_\sigma + \sum_{nk\sigma} T^r_{nk\sigma} a^+_{rnk\sigma} c_\sigma + \text{h.c.} \tag{7}$$

where $T^l_{nk\sigma}$ and $T^r_{nk\sigma}$ are the tunnelling matrix elements and it has been additionally assumed that the electron spin is conserved in the tunnelling processes.

To find tunnelling current we apply the nonequilibrium Green function method [21–25]. Accordingly, we introduce the retarded,

$$G^r_\sigma(t_1, t_2) \equiv \langle\langle c_\sigma(t_1); c^+_\sigma(t_2)\rangle\rangle^r = -i\theta(t_1 - t_2)\langle[c_\sigma(t_1), c^+_\sigma(t_2)]_+\rangle \tag{8}$$

and correlation (or lesser),

$$G^<_\sigma(t_1, t_2) \equiv \langle\langle c_\sigma(t_1); c^+_\sigma(t_2)\rangle\rangle^< = i\langle c^+_\sigma(t_2) c_\sigma(t_1)\rangle \tag{9}$$

Green functions for $\sigma = \uparrow$ and $\downarrow$. Since we consider only colinear configurations and the electron spin is conserved in tunnelling processes, it is sufficient to introduce the Green functions for each spin separately. However, the Green functions for opposite spin orientations are not independent, due to electron correlations at the dot. In the above equations electron spin ($\sigma = \uparrow$ and $\downarrow$) refers to a global quantization axis. Reversal of the magnetic moment of αth electrode is equivalent to interchanging the majority and minority electrons. Thus, if $\sigma = \uparrow$ corresponds to the majority electrons, then after magnetization reversal $\sigma = \uparrow$ corresponds to the minority ones.

In the steady state the Green functions depend only on the time difference $t_1 - t_2$, so it is more convenient to introduce their Fourier transforms, $G^r_\sigma(\epsilon) \equiv \langle\langle c_\sigma; c^+_\sigma\rangle\rangle^r_\epsilon$ and $G^<_\sigma(\epsilon) \equiv \langle\langle c_\sigma; c^+_\sigma\rangle\rangle^<_\epsilon$.

Knowledge of the Green functions allows one to calculate basic characteristics of the system out of equilibrium. First, the occupation numbers n_σ are given by $n_\sigma(t) = -iG^<_\sigma(t, t) \equiv \langle\langle c_\sigma(t); c^+_\sigma(t)\rangle\rangle^<_\epsilon$, or in the stationary state by

$$n_\sigma = \int \frac{d\epsilon}{2\pi} \text{Im}\, \langle\langle c_\sigma; c^+_\sigma\rangle\rangle^<_\epsilon. \tag{10}$$

Second, one can also calculate electric current J_σ. A general expression for tunnelling current was derived by Jauho *et al* [22]. In our case the stationary current can be written as

$$J_\sigma = \frac{ie}{2\hbar} \int \frac{d\epsilon}{2\pi} \Big\{ \big[\Gamma^l_\sigma(\epsilon) - \Gamma^r_\sigma(\epsilon)\big] \langle\langle c_\sigma; c^+_\sigma\rangle\rangle^<_\epsilon + \big[f_l(\epsilon)\Gamma^l_\sigma(\epsilon) - f_r(\epsilon)\Gamma^r_\sigma(\epsilon)\big] \times \big[\langle\langle c_\sigma; c^+_\sigma\rangle\rangle^r_\epsilon - \langle\langle c_\sigma; c^+_\sigma\rangle\rangle^a_\epsilon\big] \Big\} \tag{11}$$

where $f_l(\epsilon)$ and $f_r(\epsilon)$ are the Fermi distribution functions in the left and right electrodes, respectively, $\langle\langle c_\sigma; c^+_\sigma\rangle\rangle^a_\epsilon$ is the advanced Green function, and Γ^l_σ and Γ^r_σ describe contributions to the half-width of the level due to tunnelling through the left and right barriers, respectively,

$$\Gamma^\alpha_\sigma(\epsilon) = 2\pi \sum_{nk} |T^\alpha_{nk\sigma}|^2 \delta(\epsilon - \epsilon^\alpha_{nk\sigma}) \tag{12}$$

for $\alpha = l$ and r.

As shown by Jauho *et al* [22], equation (11) can be simplified further when $\Gamma^l_\sigma(\epsilon)$ and $\Gamma^r_\sigma(\epsilon)$ are proportional, $\Gamma^l_\sigma(\epsilon) = \lambda\Gamma^r_\sigma(\epsilon)$. In that case, one can write

$$J_\sigma = \frac{ie}{\hbar} \int \frac{d\epsilon}{2\pi} [f_l(\epsilon) - f_r(\epsilon)] \frac{\Gamma^r_\sigma(\epsilon)\Gamma^l_\sigma(\epsilon)}{\Gamma^r_\sigma(\epsilon) + \Gamma^l_\sigma(\epsilon)} \big[\langle\langle c_\sigma; c^+_\sigma\rangle\rangle^r_\epsilon - \langle\langle c_\sigma; c^+_\sigma\rangle\rangle^a_\epsilon\big]. \tag{13}$$

Equation (13) is also valid when the constant λ is spin dependent. In the following we assume that $\Gamma^l_\sigma(\epsilon)$ and $\Gamma^r_\sigma(\epsilon)$ are constant, i.e. independent of energy, $\Gamma^\alpha_\sigma(\epsilon) = \Gamma^\alpha_\sigma$ for $\alpha = l, r$.

The main point now is to find the Green functions which enter equations for the occupation numbers and electric current. For noninteracting dots (vanishing U) this can be done relatively easily in terms of the Dyson equation and self-energy. The situation is more complex for interacting dots (nonvanishing U). In that case one can use the method which takes into account both Dyson equation and equation of motion techniques [24].

Equation of motion for the retarded and lesser Green functions has the form

$$\epsilon\langle\langle c_\sigma; c_\sigma^+\rangle\rangle_\epsilon^{\mathrm{r}} = \langle[c_\sigma, c_\sigma^+]\rangle + \langle\langle[c_\sigma, H]; c_\sigma^+\rangle\rangle_\epsilon^{\mathrm{r}} \tag{14}$$

$$\epsilon\langle\langle c_\sigma; c_\sigma^+\rangle\rangle_\epsilon^{<} = \langle\langle[c_\sigma, H]; c_\sigma^+\rangle\rangle_\epsilon^{<} \tag{15}$$

which gives

$$(\epsilon - E_\sigma)\langle\langle c_\sigma; c_\sigma^+\rangle\rangle_\epsilon^{\mathrm{r}} = 1 + \sum_{nk}\sum_{\alpha=l,r} T_{nk\sigma}^{\alpha\star}\langle\langle a_{\alpha nk\sigma}; c_\sigma^+\rangle\rangle_\epsilon^{\mathrm{r}} + U\langle\langle c_\sigma c_{-\sigma}^+ c_{-\sigma}; c_\sigma^+\rangle\rangle_\epsilon^{\mathrm{r}} \tag{16}$$

$$(\epsilon - E_\sigma)\langle\langle c_\sigma; c_\sigma^+\rangle\rangle_\epsilon^{<} = \sum_{nk}\sum_{\alpha=l,r} T_{nk\sigma}^{\alpha\star}\langle\langle a_{\alpha nk\sigma}; c_\sigma^+\rangle\rangle_\epsilon^{<} + U\langle\langle c_\sigma c_{-\sigma}^+ c_{-\sigma}; c_\sigma^+\rangle\rangle_\epsilon^{<}. \tag{17}$$

The new Green functions can be found following the method described in [24]. Accordingly, the Green functions $\langle\langle a_{\alpha nk\sigma}; c_\sigma^+\rangle\rangle_\epsilon^{\mathrm{r}}$ and $\langle\langle a_{\alpha nk\sigma}; c_\sigma^+\rangle\rangle_\epsilon^{<}$ can be found from the appropriate Dyson equation. On the other hand, the Green functions $\langle\langle c_\sigma c_{-\sigma}^+ c_{-\sigma}; c_\sigma^+\rangle\rangle_\epsilon^{\mathrm{r}}$ and $\langle\langle c_\sigma c_{-\sigma}^+ c_{-\sigma}; c_\sigma^+\rangle\rangle_\epsilon^{<}$ can be calculated by writing the appropriate equations of motion, followed by a decoupling procedure to close the system of equations. In this paper we restrict our considerations to the Hartree–Fock approximation. For the retarded Green function one finds then,

$$\langle\langle c_\sigma; c_\sigma^+\rangle\rangle_\epsilon^{\mathrm{r}} = \frac{1 - n_{-\sigma}}{\epsilon - E_\sigma - \Sigma_{0\sigma}} + \frac{n_{-\sigma}}{\epsilon - E_\sigma - U - \Sigma_{0\sigma}} \tag{18}$$

where

$$\Sigma_{0\sigma} = -\mathrm{i}(\Gamma_\sigma^{\mathrm{l}} + \Gamma_\sigma^{\mathrm{r}})/2. \tag{19}$$

Similarly, one finds

$$\langle\langle c_\sigma; c_\sigma^+\rangle\rangle_\epsilon^{<} = -\frac{f_{\mathrm{l}}(\epsilon)\Gamma_\sigma^{\mathrm{l}}(\epsilon) + f_{\mathrm{r}}(\epsilon)\Gamma_\sigma^{\mathrm{r}}(\epsilon)}{\Gamma_\sigma^{\mathrm{l}}(\epsilon) + \Gamma_\sigma^{\mathrm{r}}(\epsilon)}\big[\langle\langle c_\sigma; c_\sigma^+\rangle\rangle_\epsilon^{\mathrm{r}} - \langle\langle c_\sigma; c_\sigma^+\rangle\rangle_\epsilon^{a}\big]. \tag{20}$$

The condition for the electrostatic potential of the dot can be rewritten as

$$e\left(\int \frac{\mathrm{d}\epsilon}{2\pi}\sum_\sigma \langle\langle c_\sigma; c_\sigma^+\rangle\rangle_\epsilon^{<} - \int \frac{\mathrm{d}\epsilon}{2\pi}\sum_\sigma \langle\langle c_\sigma; c_\sigma^+\rangle\rangle_\epsilon^{0<}\right) = C_{\mathrm{l}}(U_{\mathrm{e}} - U_{\mathrm{e}}^{\mathrm{l}}) + C_{\mathrm{r}}(U_{\mathrm{e}} - U_{\mathrm{e}}^{\mathrm{r}}) \tag{21}$$

where $\langle\langle c_\sigma; c_\sigma^+\rangle\rangle_\epsilon^{0<}$ is the Green function at zero bias (equilibrium situation). Equations for electric current, occupation numbers and electrostatic potential of the dot have to be solved self-consistently. Such a description is gage invariant.

3. Numerical results

Numerical calculations have been performed for two different situations; (i) the case of a non-magnetic dot and ferromagnetic electrodes, and (ii) the case of a magnetic dot coupled to one ferromagnetic and one non-magnetic electrodes. For each case the spin dependent current J_σ and average occupation number n_σ, as well as the electrostatic potential U_{e} of the dot have been calculated in a self-consistent way. We also assume that in equilibrium ($V = 0$) the chemical potentials in both electrodes are equal to zero. When the bias voltage V is applied, the chemical potential μ^{l} of the left electrode is shifted up by eV, $\mu^{\mathrm{l}} = eV$.

In the following all the energy parameters will be expressed in the units of U. The capacitance coefficients C_{l} and C_{r} are treated as free parameters and the calculations are performed for $e^2/C_{\mathrm{l}} = e^2/C_{\mathrm{l}} = 5/6$. Apart from this, the wide-band limit is assumed and Γ_σ^α ($\alpha = r, l$) are treated as parameters.

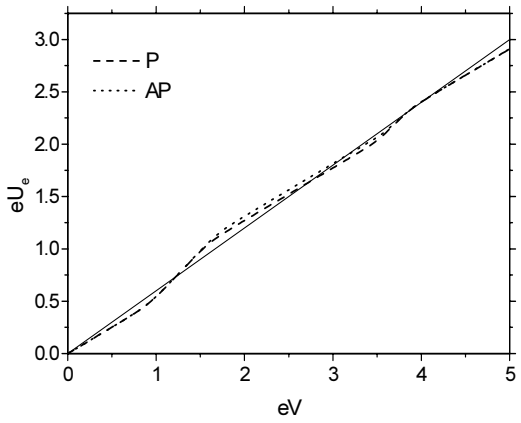

Figure 1. Electrostatic potential (eU) versus bias voltage (eV), calculated for a nonmagnetic dot in the P and AP configurations and for the parameters $e^2/C_\mathrm{l} = e^2/C_\mathrm{l} = 5/6$, $E_0 = 0.5$, $\Gamma_\mathrm{maj} = 0.015$, $\Gamma_\mathrm{min} = 0.005$ and $k_\mathrm{B}T = \Gamma_\mathrm{maj}$. The solid line corresponds to $eU/eV = 0.6$.

3.1. Non-magnetic dot

The energy level of the dot is now independent of the spin orientation, $E_\sigma = E$, and the calculations are performed for $E_\sigma^0 = E_0 = 0.5$. The right (r) and left (l) electrodes are ferromagnetic and two magnetic configurations are considered—the P and AP ones. The AP configuration corresponds to reversed magnetic moment of the right (r) electrode. In the P configuration we assume $\Gamma_\uparrow^\mathrm{l} = \Gamma_\uparrow^\mathrm{r} = \Gamma_\mathrm{maj} = 0.015$ for majority electrons, and $\Gamma_\downarrow^\mathrm{l} = \Gamma_\downarrow^\mathrm{r} = \Gamma_\mathrm{min} = 0.005$ for minority electrons. This corresponds to a symmetrical case, $\Gamma_\sigma^\mathrm{l} = \Gamma_\sigma^\mathrm{r}$. In the AP configuration, on the other hand, we have $\Gamma_\uparrow^\mathrm{l} = \Gamma_\downarrow^\mathrm{r} = \Gamma_\mathrm{maj}$ and $\Gamma_\downarrow^\mathrm{l} = \Gamma_\uparrow^\mathrm{r} = \Gamma_\mathrm{min}$. The approach we use is based on the Hartree–Fock approximation, and therefore it is valid only for temperatures higher than the Kondo temperature. Therefore, it is assumed that $k_\mathrm{B}T$ is of the order of Γ_σ or larger. In numerical calculation we assume $k_\mathrm{B}T = \Gamma_\mathrm{maj}$.

In figure 1 the self-consistent electrostatic potential U_e of the dot is shown as a function of the bias voltage (more precisely, eU_e is shown versus eV). The potentials U_e in the P and AP configurations are very similar and U_e/V is close to 0.6 in a wide range of the bias voltage (the line corresponding to $U_\mathrm{e}/V = 0.6$ is also shown in figure 1). Only small deviations from the linear dependence can be observed in the indicated bias range. For larger voltages the curve turnes down and the relevant coefficient becomes equal to 0.5 instead of 0.6.

Current–voltage (I–V) characteristics and the occupation numbers for the dot are presented in figures 2 and 3 for the P and AP configurations, respectively. For both geometries we show the spin currents J_σ, the occupation numbers n_σ, as well as the total current $J = \sum_\sigma J_\sigma$ and total number of electrons $n = \sum_\sigma n_\sigma$. The I–V curves show steps typical of systems with Coulomb blockade, i.e. the current is exponentially small below a threshold voltage (first step in the I–V curves).

The currents J_σ flowing in the two spin channels are different in the P and AP geometries. For the P configuration the current $J_\uparrow$ corresponding to majority electrons is significantly larger than the current $J_\downarrow$ corresponding to minority electrons (see figure 2(a)). In the AP configuration, on the other hand, $J_\uparrow$ and $J_\downarrow$ are almost equal in the low and high voltage regimes, except the region between the two steps. We recall here, that according to our definition, in the AP configuration the spin $\sigma = \uparrow$ ($\downarrow$) corresponds to the majority (minority) electrons in the left l electrode and minority (majority) electrons in the right electrode.

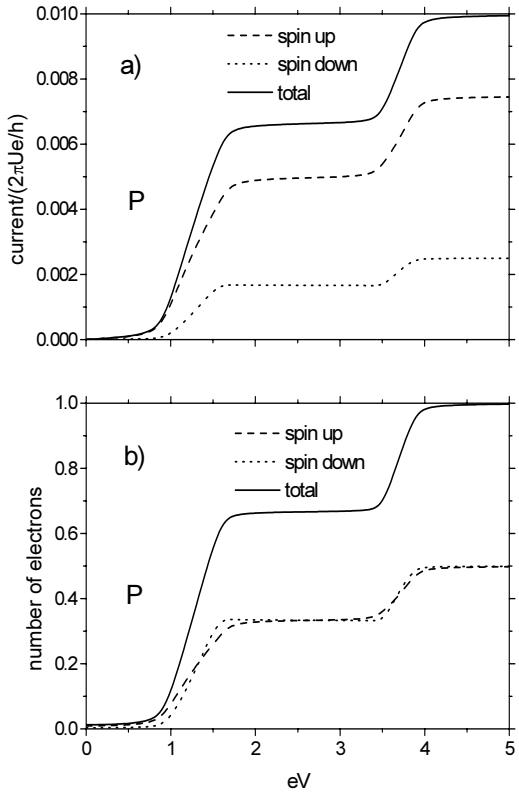

Figure 2. Electric current (a) and occupation numbers (b) as a function of the bias voltage, calculated for the P configuration. The parameters are the same as in figure 1.

For $eV \geqslant 1$, the currents $J_\uparrow$ and $J_\downarrow$ increase relatively fast with increasing bias voltage. The increase in current is accompanied by a similar increase in the occupation numbers. Both electric current and occupation numbers increase because the dot energy E crosses the chemical potential μ^1 of the left (source) electrode, and therefore the level becomes fully active in electronic transport. In the AP configuration, the increase for $n_\uparrow$ and $J_\uparrow$ is larger than the corresponding increase for $n_\downarrow$ and $J_\downarrow$.

When the bias voltage reaches values corresponding to the situation when E is well below and $E+U$ is well above the chemical potential μ^1 of the left electrode, the occupation numbers and also electric currents remain almost constant. When, however, $E + U$ approaches the chemical potential μ^1, the occupation numbers and electric current increase again and then become constant when the bias voltage increases further. In the AP configuration, the increase for $n_\downarrow$ and $J_\downarrow$ is larger than the corresponding increase for $n_\uparrow$ and $J_\uparrow$—just opposite to the situation at the first step.

In the AP configuration the matrix elements for tunnelling of electrons with spin $\uparrow$ out of the dot through the right barrier are rather small (this spin direction corresponds to minority electrons in the right electrode). On the other hand, the matrix elements for tunnelling of electrons with spin $\uparrow$ to the dot through the left barrier are large (the majority electrons in the l electrode). Consequently, the occupation number $n_\uparrow$ of the dot is larger than $n_\downarrow$ (figure 3). The quantum dot becomes then magnetized on average in the AP configuration, $n_\uparrow > n_\downarrow$. The magnetic moment of the dot, defined as $m = n_\uparrow - n_\downarrow$, increases rapidly with V at the first step

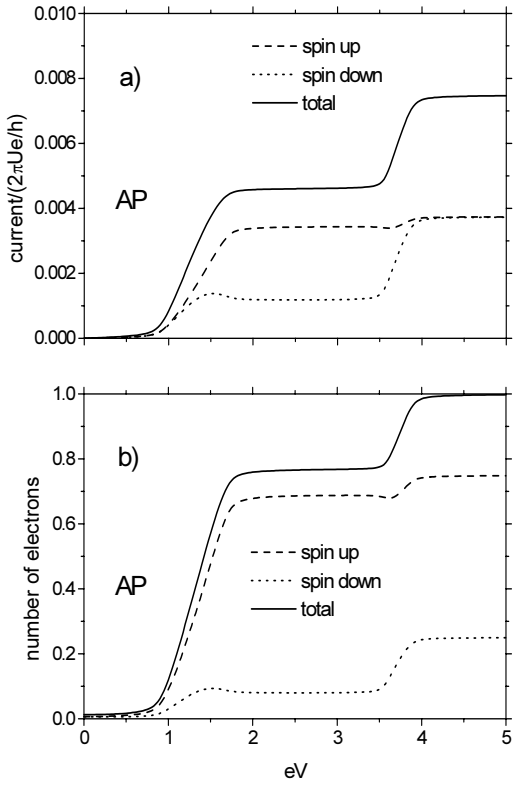

Figure 3. The same as in figure 2, but for the AP configuration.

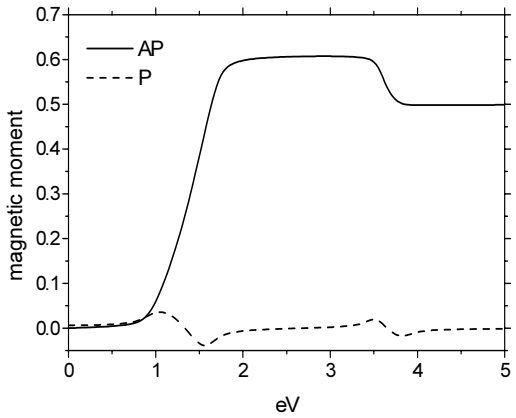

Figure 4. Magnetic moment of the dot versus bias voltage in both magnetic configurations. The parameters are the same as in figure 1.

in the I–V curves, as one can see in figure 4. Between the steps the magnetic moment remains roughly constant and then slightly decreases when V exceeds the value corresponding to the second step in the I–V characteristics. On the other hand, the average magnetic moment of the dot is close to zero in the P configuration (figures 2(b) and 4).

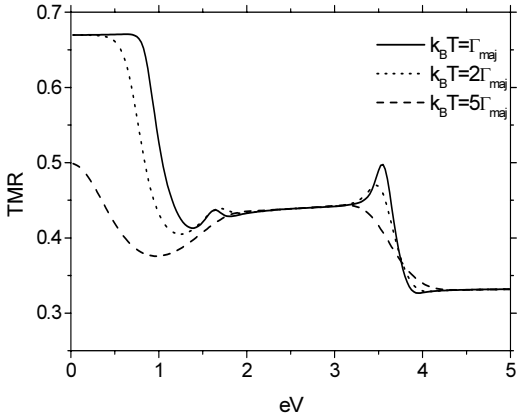

Figure 5. TMR as a function of the bias voltage, calculated for indicated temperatures. The other parameters are as in figure 1.

The difference in I–V curves for the P and AP configurations leads to TMR effect, which is defined quantitatively as TMR$= (I^{\mathrm{P}} - I^{\mathrm{AP}})/I^{\mathrm{AP}}$, where I^{P} and I^{AP} denote the tunnelling current in the P and AP configurations, respectively. Variation of TMR with the bias voltage is shown in figure 5 for three different values of the temperature. At low temperatures the TMR value is relatively high at low voltages, where electric current is exponentially suppressed, i.e. below the threshold voltage. However, it decreases at the threshold voltage, and further decreases again at the voltage corresponding to the second step. A local minimum and a local maximum appear at the first and second steps, respectively. Between the steps the TMR effect is roughly constant. The effect remains constant also for voltages above the second step. The main influence of increasing temperature on TMR occurs for voltages below the threshold voltage. The enhancement of TMR, found at low temperatures, disappears with increasing T. Also the local minimum and maximum are washed out for $k_{\mathrm{B}}T$ significantly larger than the level width.

3.2. Magnetic dot

Now we consider the situation when the dot and the left electrode are magnetic, whereas the right electrode is nonmagnetic ($\Gamma^{\mathrm{r}}_{\uparrow} = \Gamma^{\mathrm{r}}_{\downarrow} = 0.01$). The energy levels on the dot are spin-split and lower energy corresponds to $\sigma = \uparrow$. Numerical calculations are performed for $E_{0\uparrow} = 0.5$ and $E_{0\downarrow} = 0.6$. As before, two magnetic configurations, P and AP, are considered. In the AP geometry the magnetization of the left (l) electrode is reversed, whereas the energy structure of the dot remains unchanged. Thus, in this configuration the spin index $\sigma = \downarrow$ corresponds to the majority electrons in the left electrode. We assume that the spin dependence of $\Gamma^{\mathrm{l}}_{\sigma}$ is determined by properties of the magnetic electrode only. Thus, $\Gamma^{\mathrm{l}}_{\uparrow}$ and $\Gamma^{\mathrm{l}}_{\downarrow}$ interchange only when magnetic configuration varies from one to another.

The currents $J_{\uparrow}$ and $J_{\downarrow}$ flowing in the two spin channels, as well as the total current J are shown in figure 6 for the P configuration. Due to the spin splitting of the energy level, the tunnelling channel opens first for electrons with spin $\sigma = \uparrow$. Thus, at low voltages the total current is roughly equal to $J_{\uparrow}$. The tunnelling channel for electrons with spin $\sigma = \downarrow$ opens at higher voltages. As the bias voltage increases, the current $J_{\uparrow}$ achieves its local maximum and then slightly decreases when the level $E_{\downarrow}$ approaches the chemical potential of the left (source) electrode and becomes active in transport. A decrease of $J_{\uparrow}$ (and also $n_{\uparrow}$) is a

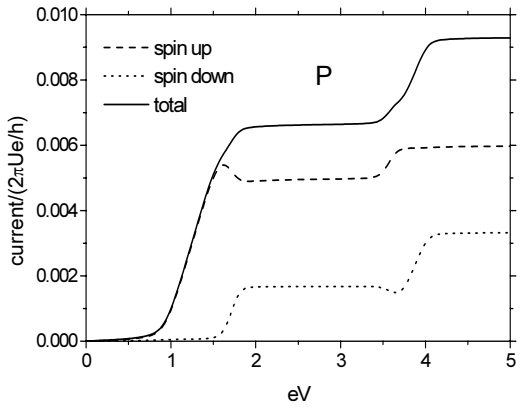

Figure 6. Current as a function of the bias voltage in the case of a magnetic dot, calculated for the P configuration and for $e^2/C_\mathrm{l} = e^2/C_\mathrm{l} = 5/6$, $E_\uparrow = 0.5$, $E_\downarrow = 0.6$ and $k_\mathrm{B}T = \Gamma_\mathrm{maj}$. Apart from this, $\Gamma_\mathrm{maj} = 0.015$ and $\Gamma_\mathrm{min} = 0.005$ for the ferromagnetic electrode, whereas $\Gamma_\uparrow = \Gamma_\downarrow = 0.01$ for the nonmagnetic electrode.

consequence of the coupling between the two spin states. Similar behaviour takes place also in the AP magnetic configuration, although there are some differences. In the P configuration the current $J_\downarrow$ remains rather small (always smaller than $J_\uparrow$). In the AP configuration, on the other hand, current in the spin-$\downarrow$ channel increases rather fast and above a certain voltage it dominates the current $J_\uparrow$. Such I–V characteristics essentially depend on the tunnelling rates between the dot and the left electrode and follow from the fact that in the P configuration $\sigma = \uparrow$ corresponds to the majority electrons, while in the AP configuration $\sigma = \uparrow$ corresponds to the minority electrons in the magnetic (left) electrode.

When the bias voltage increase further, the current in the two spin channels of both magnetic configurations remains constant. This corresponds to the situation where the level E_σ is below and $E_\sigma + U$ is above the chemical potential of the left electrode. For higher voltages the energy level $E_\uparrow + U$ approaches μ^1 and the current $J_\uparrow$ increases again. Electric current in the spin-$\downarrow$ channel decreases then slightly and reaches a local shallow minimum. When the level $E_\downarrow + U$ becomes fully active in transport, $J_\downarrow$ increases as well. Above the second steps the current remains constant again.

In the case considered now, a nonzero average magnetic moment appears on the dot in both magnetic configurations. Variation of the magnetic moment m with increasing bias voltage is presented in figure 7. When the bias increases, the magnetic moment at first increases and then decreases giving rise to a local maximum. The increase starts when the level $E_\uparrow$ crosses the Fermi level of the source electrode, which opens tunnelling channel for $\sigma = \uparrow$ electrons. When, however, the level $E_\downarrow$ enters the 'tunnelling window', the magnetic moment of the dot decreases because now electrons with $\sigma = \downarrow$ can tunnel to the dot and this diminishes the average magnetic moment. This gives rise to the first local maximum. A small difference in the positions of the maxima in P and AP configurations follows from the fact that the decrease in the AP configuration is significantly larger than in the P one. Indeed, in the AP configuration the magnetic moment after the first maximum drops to negative values, whereas in the P configuration it is positive for all voltages. When the bias increases further, another local maximum appears. This is because a new tunnelling channel opens, first for electrons with $\sigma = \uparrow$ and and then for electrons with $\sigma = \downarrow$.

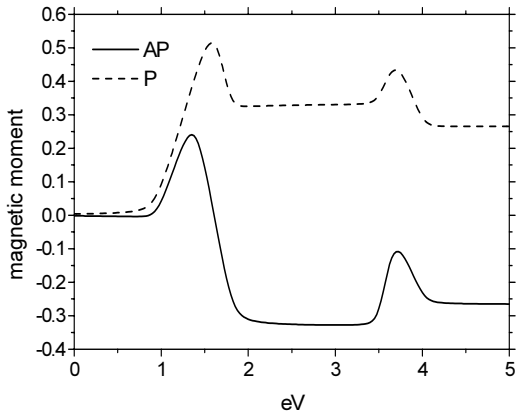

Figure 7. Magnetic moment of the dot versus bias voltage. The parameters are the same as in figure 6.

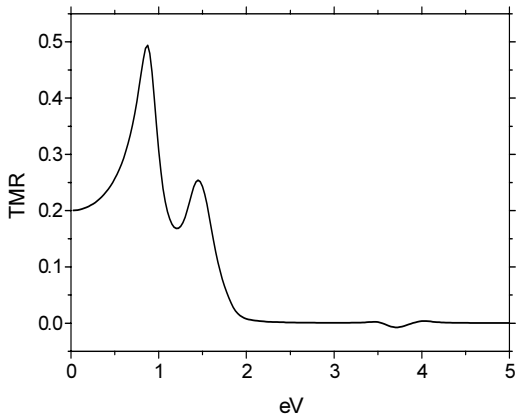

Figure 8. TMR as a function of the bias voltage, calculated for the parameters as in figure 6.

Changes in the spin polarization of the dot strongly influence the total currents flowing in the P and AP configurations, and therefore influence also TMR. Variation of TMR with the bias voltage is depicted in figure 8. At low bias, the value of TMR strongly increases showing a pronounced peak at $eV \sim 0.9$, when the level $E_\uparrow$ becomes fully active in the transport. The second, smaller peak appears when $E_\downarrow$ is close to μ^1. However, for higher voltages TMR practically drops to zero.

4. Summary and conclusions

We have considered tunnelling through nonmagnetic and magnetic quantum dots with a single discrete level in the presence of Coulomb correlation. In the case of nonmagnetic dots, both external electrodes were ferromagnetic giving rise to spin polarized transport. On the other hand, for magnetic dots only one external electrode was magnetic, whereas the second one was nonmagnetic. Two magnetic configurations were discussed—the P and AP ones. Considerations have been limited to the Hartree–Fock approximation for the dot Green function, which is reasonable for temperatures higher than the Kondo temperature.

It was shown that tunnelling magnetoresistance due to variation of the magnetic configuration from the AP to P one significantly depends on the bias voltage. The magnetoresistance is relatively large below the threshold voltage, where, however, the electric current is exponentially small. Magnitude of TMR in this bias range strongly depends on temperature and rapidly falls down with increasing T. Between the two steps in the I–V curves, the TMR effect is enhanced by Coulomb correlations. This enhancement disappears for voltages above the second step.

The considerations were restricted to single-domain magnetic electrodes. In the limit of strong tunnelling one may expect exchange coupling between ferromagnetic electrodes—similar to exchange coupling in simple planar junctions. Such a coupling may have an influence on magnetic configuration of the junction and on the domain structure in the ferromagnetic electrodes. Since in our case tunnelling takes place only through a single discrete level and the external electrodes are macroscopic, one may assume that this coupling is weaker than the coupling induced by magnetostatic dipolar interaction [28].

Acknowledgment

The work has been supported by The Polish State Committee for Scientific Research through the Research Project 5 P03B 091 20.

References

[1] Prinz G A 1999 *J. Magn. Magn. Mater.* **200** 57
[2] Daughton J M 1999 *J. Magn. Magn. Mater.* **192** 334
[3] Moodera J S, Kinder L R, Wong T M and Meservey R 1995 *Phys. Rev. Lett.* **74** 3273
[4] Parkin S S P *et al* 1999 *J. Appl. Phys.* **85** 5828
[5] Baibich M N, Broto J M, Fert A, Nguyen van Dau F, Petroff F, Etienne P, Creuzet G, Friederich A and Chazelas J 1988 *Phys. Rev. Lett.* **61** 2472
[6] Binasch G, Grünberg P, Saurenbach F and Zinn W 1989 *Phys. Rev.* B **39** 4828
Barnaś J, Fuss A, Camley R E, Grünberg P and Zinn W 1990 *Phys. Rev.* B **42** 8110
[7] Zhang X, Li B Z, Sun G and Pu F C 1997 *Phys. Rev.* B **56** 5484
Wilczyński M and Barnaś J 2000 *J. Magn. Magn. Mater.* **221** 373
[8] Barnaś J and Fert A 1998 *Phys. Rev. Lett.* **80** 1058
Barnaś J and Fert A 1998 *Europhys. Lett.* **44** 85
Barnaś J and Fert A 1999 *J. Magn. Magn. Mater.* L **192** 391
[9] Takahashi S and Maekawa S 1998 *Phys. Rev. Lett.* **80** 1758
[10] Brataas A, Nazarov Yu V, Inoue J and Bauer G E W 1999 *Eur. Phys. J.* B **9** 421
Wang X H and Brataas A 1999 *Phys. Rev. Lett.* **83** 5138
[11] Imamura H, Chiba J, Mitani S, Takanashi K, Takahashi S, Maekawa S and Fujimori H 2000 *Phys. Rev.* B **61** 46
[12] Yakushiji K, Mitani S, Takanashi K, Takahashi S, Maekawa S, Imamura H and Fujimori H 2001 *Appl. Phys. Lett.* **78** 515
[13] For a review see Grabert H and Devoret M H (ed) 1992 *Single Charge Tunneling (NATO ASI Series vol 294)* (New York: Plenum)
Averin D V and Likharev K K 1986 *J. Low Temp. Phys.* **62** 345
[14] Averin D V, Korotkov A N and Likhariev K K 1991 *Phys. Rev.* B **44** 6199
Beenakker C W J 1991 *Phys. Rev.* B **44** 1646
[15] Ralph D C, Gueron S, Black C T and Tinkham M 2000 *Physica* B **280** 420
[16] Barnaś J, Martinek J, Michałek G, Bułka B and Fert A 2000 *Phys. Rev.* B **62** 12 363
Martinek J, Barnaś J, Michałek G, Bułka B R and Fert A 1999 *J. Magn. Magn. Mater.* L **207** 1
[17] Bułka B R 2000 *Phys. Rev.* B **62** 1186
[18] Rudziński W and Barnaś J 2001 *Phys. Rev.* B **64** 085318
[19] Wang B, Wang J and Guo H 1999 *J. Appl. Phys.* **86** 5094
[20] Glazman L I and Matveev K A 1988 *Pis. Zh. Eksp. Teor. Fiz.* **48** 403 (Engl. transl. 1988 *JETP Lett.* **48** 445)
[21] Groshev A, Ivanov T and Valtchinov V 1991 *Phys. Rev. Lett.* **66** 1082

[22] Jauho A P, Wingreen N S and Meir Y 1994 *Phys. Rev.* B **50** 5528
[23] Kang K and Min B I 1995 *Phys. Rev.* B **52** 10 689
[24] Niu C, Liu L and Lin T 1995 *Phys. Rev.* B **51** 5130
[25] Pals P and MacKinnon A 1996 *J. Phys.: Condens. Matter* **8** 5401
[26] Glazman L I and Raikh M E 1988 *Pis. Zh. Eksp. Teor. Fiz.* **47** 378 (Engl. transl. 1988 *JETP Lett.* **47** 452)
Ng T K and Lee P A 1988 *Phys. Rev. Lett.* **61** 1768
[27] Goldhaber-Gordon D *et al* 1998 *Nature* **391** 156
Inoshita T 1998 *Science* **281** 525
Cronenwett S M, Oosterkamp T H and Kouwenhoven L 1998 *Science* **281** 540
[28] Schrag B D, Anguelouch A, Xiao G, Trouilloud P, Lu Y, Gallagher J and Parkin S S P 2000 *J. Appl. Phys.* **87** 4682